Approaching the true ground state of frustrated *A*-site spinels: A combined magnetization and polarized neutron scattering study

Harikrishnan S. Nair,[1,*] Zhendong Fu,[2] Jörg Voigt,[1] Yixi Su,[2] and Th. Brückel[1,2]

[1]*Jülich Center for Neutron Sciences JCNS and Peter Grünberg Institute PGI,*
JARA-FIT, Forschungszentrum Jülich GmbH, 52425 Jülich, Germany
[2]*Jülich Center for Neutron Sciences JCNS, Outstation at MLZ, Forschungszentrum Jülich GmbH,*
Lichtenberg Straße 1, D-85747 Garching, München, Germany

We re-investigate the magnetically frustrated, *diamond-lattice-antiferromagnet* spinels $FeAl_2O_4$ and $MnAl_2O_4$ using magnetization measurements and diffuse scattering of polarized neutrons. In $FeAl_2O_4$, macroscopic measurements evidence a "cusp" in zero field-cooled susceptibility around 13 K. Dynamic magnetic susceptibility and *memory effect* experiments provide results that do not conform with a canonical spin-glass scenario in this material. Through polarized neutron-scattering studies, absence of long-range magnetic order down to 4 K is confirmed in $FeAl_2O_4$. By modeling the powder averaged differential magnetic neutron-scattering cross section, we estimate that the spin-spin correlations in this compound extend up to the third nearest-neighbor shell. The estimated value of the Landé *g* factor points towards orbital contributions from Fe^{2+}. This is also supported by a Curie-Weiss analysis of the magnetic susceptibility. $MnAl_2O_4$, on the contrary, undergoes a magnetic phase transition into a long-range ordered state below $\approx$40 K, which is confirmed by macroscopic measurements and polarized neutron diffraction. However, the polarized neutron studies reveal the existence of prominent spin fluctuations co-existing with long-range antiferromagnetic order. The magnetic diffuse intensity suggests a similar short-range order as in $FeAl_2O_4$. Results of the present work support the importance of spin-spin correlations in understanding magnetic response of frustrated magnets like *A*-site spinels which have predominant short-range spin correlations reminiscent of the "spin-liquid" state.

DOI: 10.1103/PhysRevB.89.174431
PACS number(s): 75.25.−j, 75.30.Et, 75.50.−y

I. INTRODUCTION

AB_2X_4 ($A =$ Mn, Fe, Co; $B =$ Al, Sc; $X =$ O, S) spinels are frustrated magnets which exhibit spin liquid [1], orbital liquid [2], or orbital glass [3] states that arise from magnetic frustration effects. In *A*-site spinels, where the magnetic atom occupies the tetrahedrally coordinated *A* site and forms a diamond lattice, frustration arises from competing nearest-neighbor (NN) and next-nearest neighbor (NNN) exchange interactions [1–4]. This scenario is different from the case of *B*-site spinels where the magnetic atoms form a pyrochlore-type lattice and hence the observed frustration effects are inherently geometric in nature. Ideally, a diamond-lattice antiferromagnet with only NN coupling J_1 is not magnetically frustrated. Additional interactions in the form of NNN couplings, J_2, are necessary to create frustration. Monte Carlo (MC) simulations based on the "order by disorder" [5] scenario in diamond-lattice antiferromagnets predict that exotic phases like a *spiral spin liquid* are realized for $(\frac{J_2}{J_1}) > \frac{1}{8}$ [6]. The experimental verification of *spiral spin liquid* in this class of materials is still lacking. In the Al-based *A*-site spinel series, $CoAl_2O_4$ has been investigated in detail as a promising candidate for the order by disorder physics. However, existing literature on $CoAl_2O_4$ is contradictory—an early report by Roth predicts an antiferromagnetic (AFM) ground state [7]; Krimmel *et al.,* showed a liquidlike magnetic structure factor [1] and Tristan *et al.,* suggested spin-glass-like physics [4]. Recent neutron-diffraction studies combined with MC simulations confirm the ground state to be AFM and the phase above T_N to be a

"spin liquid" [8]. The magnetic ground state of $FeAl_2O_4$ is reported to be similar to that of $CoAl_2O_4$ with predominantly spin-glass-like features [4]. On the other hand, $MnAl_2O_4$ shows long-range magnetic order below $T_N \approx 45$ K [1,4]. The existing reports on (Fe, Mn)Al_2O_4 more or less confirm spin-glass-like character for the Fe spinel while the Mn compound is described as an antiferromagnet. However, being in close proximity to the spin-liquid' system $CoAl_2O_4$ in terms of the energy scales (comparable Curie-Weiss temperatures), it is worthwhile to re-investigate the Fe and Mn spinels in order to probe their physics in detail, keeping in mind that the nature of short-range magnetic correlations or the exact magnetic ground state of these systems are not unambiguously determined. In this paper we focus on the study of spin-spin correlations in $FeAl_2O_4$ and $MnAl_2O_4$. Our experiments bring us closer to the true ground state of these frustrated magnets: we show that in $FeAl_2O_4$ short-range magnetic order prevails and it does not form a canonical spin glass, we determine the magnetic structure of the long-range ordered phase in $MnAl_2O_4$ and show that short- and long-range order coexist in this material.

II. EXPERIMENTAL DETAILS

The polycrystalline samples used in the present investigation were prepared through solid-state synthesis routes following a prescription reported earlier [1]. This protocol of synthesis adopts a slow cooling rate for synthesis and thereby minimizes cation inversion. The cooling rates adopted for our samples were 15–10 C/h. The synthesized samples were characterized by laboratory x rays using a Huber G670

---

*h.nair@fz-juelich.de

diffractometer with monochromatic Cu-$K\alpha$ radiation. Magnetic measurements in field-cooled (FC) and zero field-cooled (ZFC) modes were carried out on polycrystalline pellets in a commercial superconducting quantum interference device magnetic property measurement system (MPMS, Quantum Design Inc.) using the ultralow field option and also using the vibrating sample magnetometer (VSM) option of physical property measurement system (PPMS, Quantum Design Inc.). The protocol for *memory effect* reported by Mathieu *et al.* [9] was followed to search for a possible spin-glass phase in FeAl$_2$O$_4$. Neutron-diffraction patterns with polarized neutrons and polarization analysis were recorded at the diffuse neutron spectrometer (DNS) [10] at the MLZ in Garching, Germany. Using XYZ polarization analysis [11] the coherent nuclear, the spin-incoherent, and the magnetic scattering can be separated. The wavelength of incident neutrons was $\lambda = 4.2$ Å leading to a maximal scattering vector magnitude of $\mathbf{Q} = 2.67$ Å^{-1}. Due to the long neutron wavelength, only a small portion of reciprocal space can be probed. Rietveld refinements [12] of the x-ray and neutron powder diffraction data were performed using FULLPROF suite program [13]. The software SARAh [14] was used for magnetic structure determination using representational analysis.

III. RESULTS

A. Crystal structure: FeAl$_2$O$_4$ and MnAl$_2$O$_4$

The powder-diffraction patterns of FeAl$_2$O$_4$ and MnAl$_2$O$_4$ are shown in Figs. 1(a) and 1(b) respectively. Rietveld refinement of the data yield a lattice constant value of a(Å) $= 8.1582(4)$ for FeAl$_2$O$_4$ and $8.2097(2)$ for MnAl$_2$O$_4$ respectively, which are comparable to reported values [4]. The results of Rietveld refinement for both spinels are shown in Fig. 1. In a "normal" AB_2X_4 spinel with cubic $Fd\bar{3}m$ (227) space group, A occupies the Wyckoff position $8a$ ($\frac{1}{8}, \frac{1}{8}, \frac{1}{8}$);
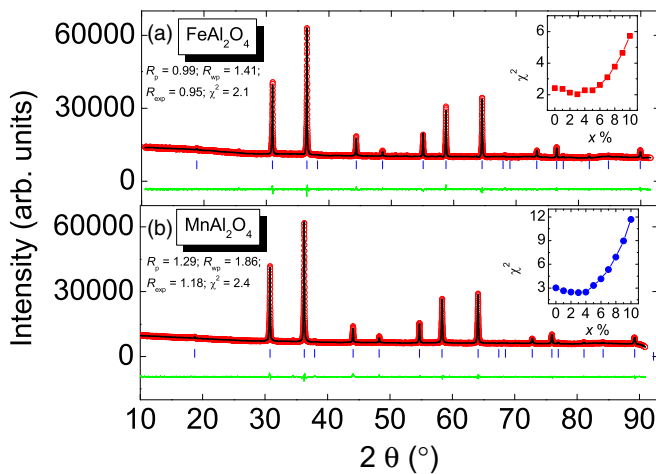
B occupies $16d$ ($\frac{1}{2}, \frac{1}{2}, \frac{1}{2}$), and oxygen occupies $32e$ (u, u, u) where $u = 0.25$. The refined value of $u = 0.2644(2)$ obtained in the present case for FeAl$_2$O$_4$ deviates from the ideal spinel value but is comparable with previous reports claiming a low degree of inversion [4]. In order to ascertain the percentage of cation inversion, refinement of the x-ray data was carried out assuming the stoichiometric formula $(A_{1-x}Al_x)[Al_{2-x}A_x]O_4$ ($A =$ Fe, Mn) where x is the inversion parameter. During the Rietveld fit of the x-ray data, the parameters that were varied are the zero-point shift, scale factor, background, profile parameters, lattice parameters, oxygen position, and the inversion parameter. The Debye-Waller factors were fixed at isotropic values obtained from powder-diffraction studies on similar spinels [15]. A value of the order of $x = 0.02(3)$ was obtained suggesting that the degree of inversion is insignificant. The Rietveld refinements were performed to test for the best value of χ^2 by varying the degree of inversion from $x = 0$ to 1. The results obtained in this way support the low content of inversion in the samples and are presented as insets of Figs. 1(a) and 1(b)
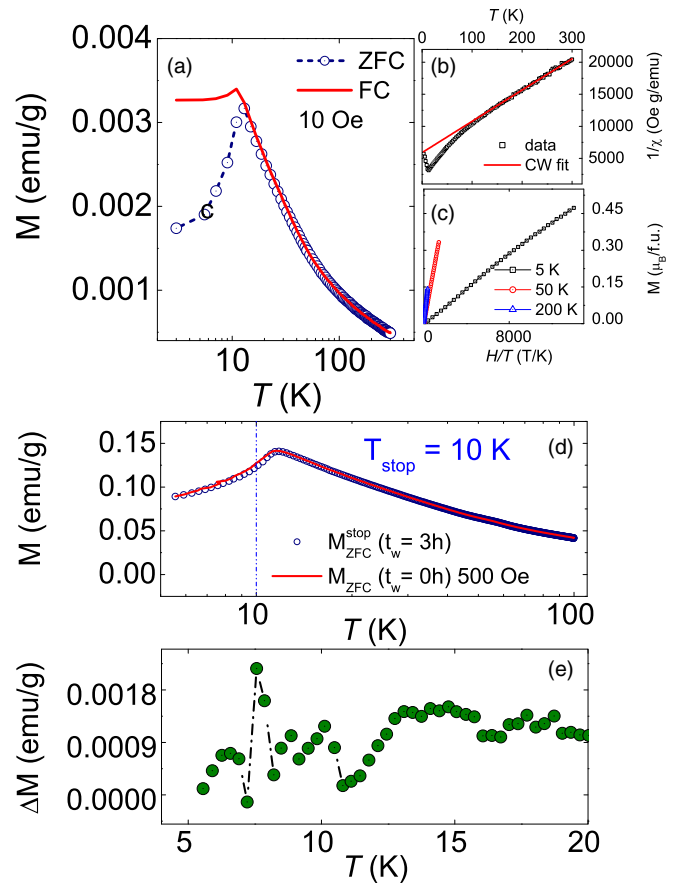

FIG. 2. (Color online) (a) ZFC and FC magnetization curves for FeAl$_2$O$_4$ show a magnetic anomaly at $T_a \approx 13$ K. Panel (b) shows the plot of $1/\chi(T)$ and the CW fit which starts to deviate close to 100 K. Panel (c) shows that the scaling of M versus H/T deviates at low temperature ruling out the presence of superparamagnetic clusters. (d) The ZFC *memory effect* experiment with a T_{stop} at 10 K to test the spin-glass phase in FeAl$_2$O$_4$. (e) Shows the difference between the two ZFC curves in (d) which, ideally, should display a significant peak at T_{stop} if canonical spin-glass phase was present. The error bars were comparable to the size of data points.

FIG. 1. (Color online) The powder x-ray diffractograms of (a) FeAl$_2$O$_4$ and (b) MnAl$_2$O$_4$ along with Rietveld refinement fits. Both the compounds are refined in cubic $Fd\bar{3}m$ space group. The reliability factors of the refinements are indicated in the graphs. The insets of (a) and (b) show the variation of goodness of fit with cationic inversion parameter x for FeAl$_2$O$_4$ and MnAl$_2$O$_4$ respectively.

for FeAl$_2$O$_4$ and MnAl$_2$O$_4$ respectively. Within the resolution of the observed data, no residues of unreacted oxides of Fe or Mn were traceable, however an unidentified weak signal at $2\Theta \sim 26°$ is observed in the case of FeAl$_2$O$_4$. The magnetic measurements which are presented later on do not lead to suspicion about major magnetic impurities in the samples. In Fig. 2(a), which shows the ZFC and FC magnetization curves for FeAl$_2$O$_4$, a magnetic anomaly is evident at 13 K, where the curves bifurcate. The magnetic susceptibility at high temperature was analyzed using the Curie-Weiss expression, $\chi(T) = \frac{\mu_B^2}{3k_B}\left(\frac{g_{eff}^2 S(S+1)}{T-\Theta}\right)$ leading to an effective paramagnetic moment, $\mu_{eff} = g_{eff}\sqrt{S(S+1)} \approx 5.3(4)\ \mu_B/$f.u. and Curie-Weiss temperature, $\Theta_{CW} = -120(1)$ K. The effective paramagnetic moment is comparable to the spin-only moment value $4.9\mu_B/$f.u. for Fe^{2+} ($3d^6$; $S = 2$; $L = 2$). Slight differences in the effective moment value in the case of FeAl$_2$O$_4$ have been attributed to the orbital degrees of freedom pertaining to Fe^{2+} [1,4].

Previous reports of bulk magnetic properties, neutron diffraction, and Mössbauer spectroscopy have attributed the observed anomalies to a spin-glass or spin-glass-like phase in FeAl$_2$O$_4$ [4,16]. The plot of inverse magnetic susceptibility and Curie-Weiss (CW) fit are presented in Fig. 2(b) which shows deviation from linear behavior close to 100 K itself, signifying that the spin correlations extend to high temperatures. In Fig. 2(c), a scaling of M versus H/T at three different temperatures, derived from the isothermal magnetization plots, is presented. At low temperatures below the T_a, a perfect scaling is not observed thus ruling out the possibility that FeAl$_2$O$_4$ could be a system of noninteracting paramagnetic clusters [17].

In order to ascertain whether a genuine canonical spin-glass phase is present, we performed *memory effect* experiments. In this experiment, initially a ZFC curve M_{zfc} was recorded in the warming cycle at constant rate of heating. Next, the sample was zero-field cooled to $T_{stop} = 10$ K $< T_a$ and held constant for $t_w = 3$ h; afterwards the sample was cooled to the lowest temperature. Finally, the magnetization M_{zfc}^{stop} was measured while warming the sample at the same constant rate as done for M_{zfc}. The resulting magnetization curves are presented in Fig. 2(d). For canonical spin-glass materials, the difference between these two curves, i.e., $\Delta M = (M_{zfc} - M_{zfc}^{stop})$ should present a peak centered at the temperature at which the halt was administered (i.e., T_{stop}) [9]. The ΔM for FeAl$_2$O$_4$ presented in Fig. 2(e) does not support a canonical spin-glass state. The *memory effect* experiment was repeated for lower values of applied fields of 50 and 100 Oe which also did not present "memory." The *memory effect* in canonical spin glasses can be described based on hierarchical organization of metastable states as a function of temperature which attempts to explain the effect based on a phase-space picture where the free-energy barriers grow as temperature is reduced [18]. Equivalently, a real-space picture of "droplets" of spins can also be used [19]. Below the spin-glass transition, the "droplet picture" assumes the presence of only one phase and its spin-reversed counterpart but the spins arrange randomly as dictated by the disordered nature of interactions and effect of temperature. Though the spinel compounds investigated in the present work are frustrated, the lack of site disorder
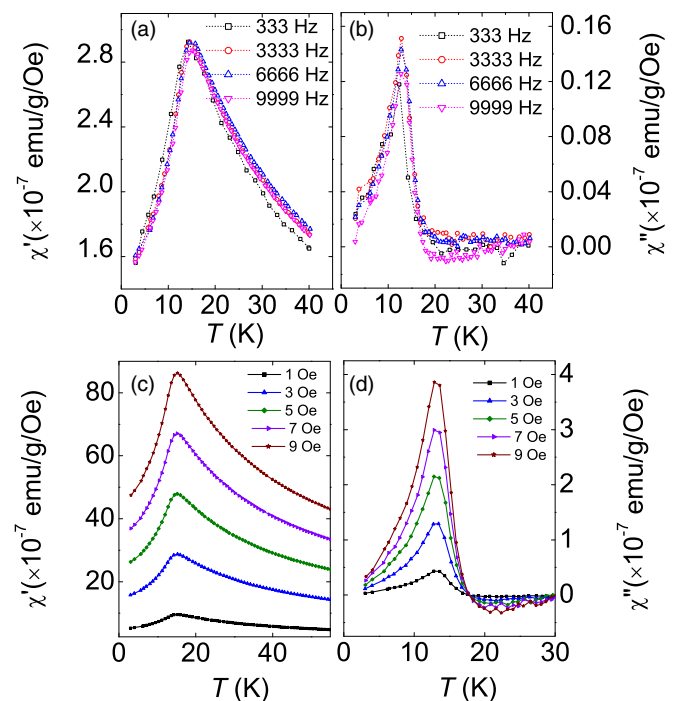

FIG. 3. (Color online) Real (a) and imaginary (b) parts of ac susceptibility, $\chi(T)$, of FeAl$_2$O$_4$ at various frequencies. No significant frequency dependence of T_a is observed. Real (c) and imaginary (d) parts of $\chi(T)$ at 9999 Hz with increasing dc amplitude of measuring ac field. For the sake of clarity, only the curves at 2-Oe interval are shown.

reduces the probability of formation of a true spin-glass phase.

ac susceptibility experiments on FeAl$_2$O$_4$ also do not support a spin-glass-like phase. The real and imaginary parts of ac susceptibility at different frequencies in the range 333 to 9999 Hz presented in Figs. 3(a) and 3(b) do not show frequency-dependent shifts of T_a which is a typical feature of spin glasses. Crucial features of the spin-glass state are the presence of relaxation processes of all time scales and aging. The signature of aging is visible in the real and imaginary parts of ac susceptibility where the susceptibility relaxes down. Moreover, for a canonical spin-glass transition, dynamical scaling holds near the critical temperature and hence susceptibility should obey critical scaling. Then, the apparent spin-glass transition temperatures at finite frequencies as fixed by the peak of ac susceptibility curves must obey a power law [20]. These features are absent in the ac susceptibility of FeAl$_2$O$_4$. Increasing the dc amplitude of the ac measuring field only enhances the magnetic susceptibility, typical of antiferromagnets; Figs. 3(c) and 3(d).

B. Polarized neutron scattering: FeAl$_2$O$_4$

1. Short-range spin correlations

From the macroscopic magnetic measurements, it is clear that FeAl$_2$O$_4$ has a complex ground state which is not explainable within the canonical spin-glass scenario. In order to understand the observed magnetic properties and to disentangle the long- and short-range magnetic contributions,
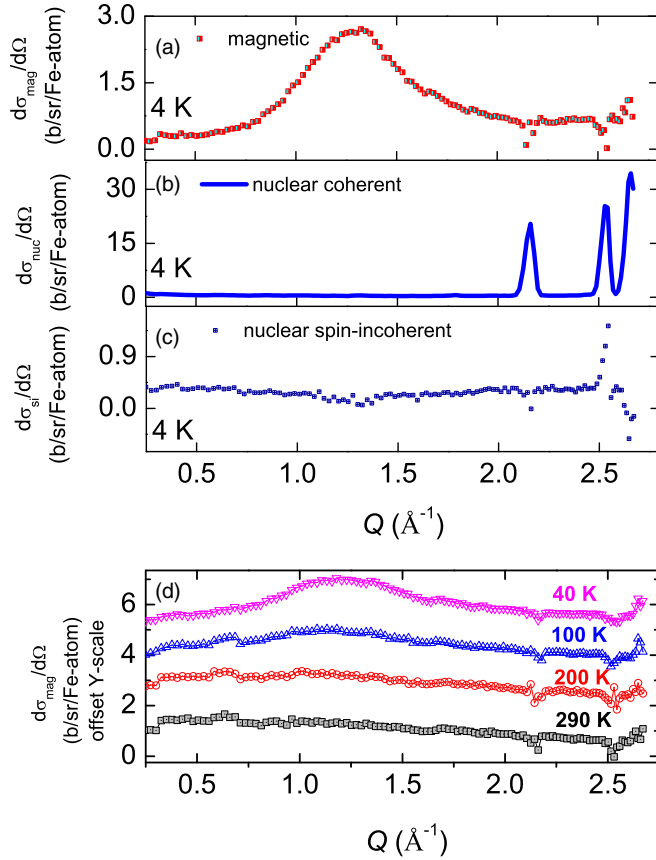
FIG. 4. (Color online) Magnetic (a), nuclear coherent (b), and nuclear spin-incoherent (c) contributions to the differential scattering cross section of $FeAl_2O_4$ at 4 K. Panel (d) shows the magnetic scattering cross sections at 40, 100, 200, and 290 K. The y-axis scale is offset by a factor of 1.2 for clarity. Polarization analysis becomes less reliable at the positions of strong nuclear reflections, which produce the scatter of data points.

spin-spin correlation functions are extremely helpful. The spin-correlation functions can be experimentally determined through the technique of polarized neutron scattering with polarization analysis which separates the nuclear and magnetic scattered intensities from the total scattered intensity. Within the quasistatic approximation, the nuclear coherent (nc), nuclear spin-incoherent (nsi), and magnetic (m) scattering cross sections are separated using the xyz polarization analysis in the *spin-flip* (SF) and *non-spin-flip* (NSF) channels [11]. The xy plane is defined by the multidetector array of DNS instrument which makes the scattering vector **Q** always perpendicular to the z direction. The SF and NSF partial differential cross sections are then ($\frac{d\sigma_{SF}^{x,y,z}}{d\Omega}$) and ($\frac{d\sigma_{NSF}^{x,y,z}}{d\Omega}$). By making suitable combinations of the expressions for cross sections, the nuclear coherent, nuclear spin-incoherent, and magnetic scattering components can be separated [11]:

$$\left(\frac{d\sigma}{d\Omega}\right)_{m.} = 2\left(\frac{d\sigma_x^{SF}}{d\Omega} + \frac{d\sigma_y^{SF}}{d\Omega} - 2\frac{d\sigma_z^{SF}}{d\Omega}\right)$$

$$= -2\left(\frac{d\sigma_x^{NSF}}{d\Omega} + \frac{d\sigma_y^{NSF}}{d\Omega} - 2\frac{d\sigma_z^{NSF}}{d\Omega}\right),$$

$$\left(\frac{d\sigma}{d\Omega}\right)_{nc.} = \left(\frac{d\sigma_z^{NSF}}{d\Omega} - \frac{1}{2}\frac{d\sigma}{d\Omega}_{m.} - \frac{1}{3}\frac{d\sigma}{d\Omega}_{nsi.}\right),$$

$$\left(\frac{d\sigma}{d\Omega}\right)_{nsi.} = \frac{3}{2}\left(3\frac{d\sigma_z^{SF}}{d\Omega} - \frac{d\sigma_x^{SF}}{d\Omega} - \frac{d\sigma_y^{SF}}{d\Omega}\right).$$

These equations hold for ideal experimental conditions for polarization and flipping ratio.

In order to obtain the absolute scattering cross sections, vanadium standard is usually measured separately in the same experimental conditions.

The results of polarized neutron-scattering experiment on $FeAl_2O_4$ are presented in Fig. 4. The magnetic (a), nuclear coherent (b), and nuclear spin-incoherent (c) contributions to differential scattering cross section at 4 K are shown separately. Figure 4(d) shows the magnetic cross sections at 40, 100, 200, and 290 K where a gradual loss of spin correlations and transition to a pure form factor square decay of the intensity with temperature is evident. The nuclear coherent scattering intensities of $FeAl_2O_4$ at 4 K as presented in Fig. 4(b), can consistently be described with the structural parameters obtained from x-ray refinements. The refined lattice parameters are comparable to the values obtained from x-ray data analysis. It is clear from Fig. 4(a) that $FeAl_2O_4$ does not enter a magnetically long-range ordered state down to 4 K. The broad and diffuse nature of the magnetic scattered intensity suggests that the spins in $FeAl_2O_4$ are correlated to each other over short distances.

In order to obtain a quantitative estimate of the spin-spin correlations in $FeAl_2O_4$, we modeled the observed spin correlations by calculating the powder averaged differential magnetic cross section [21],

$$\left(\frac{d\sigma_{mag}}{d\Omega}\right) = \frac{2}{3}\left(\frac{\gamma e^2}{mc^2}\right)^2\left(\frac{g}{2}\right)^2 S(S+1)f^2(\mathbf{Q})$$

$$\times\left[1 + \sum_{n=1}^{N}\frac{\langle S_0 \cdot S_n\rangle}{S(S+1)}c_n\frac{\sin(QR_n)}{QR_n}\right], \quad (1)$$

where $(\gamma e^2/mc^2) = 5.39$ pm is the magnetic scattering length, $f(\mathbf{Q})$ is the magnetic form factor of the Fe^{2+} ion (or Mn^{2+} in the case of $MnAl_2O_4$) [22], and R_n and c_n are the radius and coordination number of the nth near-neighbor shell respectively. The above expression is a simplified form for isotropic spin pair correlations, while the complete form contains additional terms; see [23]. The magnetic part of the differential cross-section data for $FeAl_2O_4$ at 4, 40, and 100 K were least-squares fitted as per Eq. (1). The normalized nth near-neighbor pair correlations, $\frac{\langle S_0 \cdot S_n\rangle}{S(S+1)}$, and the Landé factor g were set as adjustable fitting parameters. The initial value of S was fixed at 2 corresponding to the spin of Fe^{2+}. The fitting results are shown as solid lines in Figs. 5(a)–5(c) along with the data for 4, 40, and 100 K. The fit parameters are summarized in Tables I and II. For a comparison, the form factor of Fe^{2+} ($S = 2$) is plotted in Fig. 5. The fitting is limited to $n = 6, 5$, and 2 for temperatures 4, 40, and 100 K, respectively, as can be seen from the table. The negative and positive signs of the normalized near-neighbor pair correlations stand for the antiferromagnetic and ferromagnetic type of spin correlations, respectively. It is clear that the

TABLE I. The refined lattice constant (a), oxygen position (u), and inversion parameter (x) for $FeAl_2O_4$ and $MnAl_2O_4$ at room temperature. The goodness of fit are also represented. In the cubic $Fd\overline{3}m$ space group of AB_2X_4, A site is $8a(\frac{1}{8},\frac{1}{8},\frac{1}{8})$; B site is $16d(\frac{1}{2},\frac{1}{2},\frac{1}{2})$, and X site is $32e(u,u,u)$.

Spinel	a (Å)	u	x	χ^2
$FeAl_2O_4$	8.15826(4)	0.2644(2)	0.02(3)	2.2
$MnAl_2O_4$	8.20979(4)	0.2659(1)	0.014(4)	2.4

nearest neighbors are antiferromagnetically coupled and the next-nearest neighbors show weak ferromagnetic correlations. There exist very little correlations for $n > 3$ neighbors, but including the $n > 3$ neighbors was necessary to achieve good fits to the 4- and 40-K data. Also, we can see that the degree of correlation decreases as the temperature increases from 4 to 100 K. The Landé factor g estimated from the fit is larger than the spin-only value 2, which could be due to the orbital contribution from Fe^{2+} ions. This result may suggest an orbital contribution to the estimated effective moment as deduced from the CW analysis of the magnetic susceptibility.

The magnetic scattering intensity at different temperatures, as presented in Fig. 4, were also analyzed using Lorentzian function to model the peak function and extract the magnetic correlation length ξ. The value ξ(Å) ≈ 11 obtained is roughly three times the Fe-Fe bond distance in $FeAl_2O_4$ (≈ 3.5 Å), or, close to fifth NN distances of Fe [a preliminary estimate using the expression $\xi \approx (\frac{2\pi}{\Delta \mathbf{Q}})$, where $\Delta \mathbf{Q}$ is the full width at half maximum of the correlation peak, also gave a similar value]. In Fig. 5(d), the temperature evolution of ξ is presented, which shows that the correlation length gradually decreases with temperature. It is clear that the short-range spin-spin correlations persist to temperatures $T > T_a$.

C. Magnetization: MnAl$_2$O$_4$

The magnetization data of $MnAl_2O_4$ presented in Fig. 6 display a magnetic phase transition at ≈ 40 K. Analyzing the paramagnetic regime of the magnetization curve using the CW law, an effective paramagnetic moment $\mu_{\text{eff}} \sim 5.6(3)\mu_B$/f.u. and $\Theta_{\text{CW}} = -126(2)$ K are obtained. The experimentally obtained effective moment value is comparable to the theoretical spin-only value of Mn^{2+} ($3d^5$; $S = \frac{5}{2}$; $L = 0$), $5.9\mu_B$/f.u. The frustration parameter f for $MnAl_2O_4$ is 3.5, which is low compared to the value for $FeAl_2O_4$. Though the f value is less than half of that for $FeAl_2O_4$, the Θ_{CW} values of
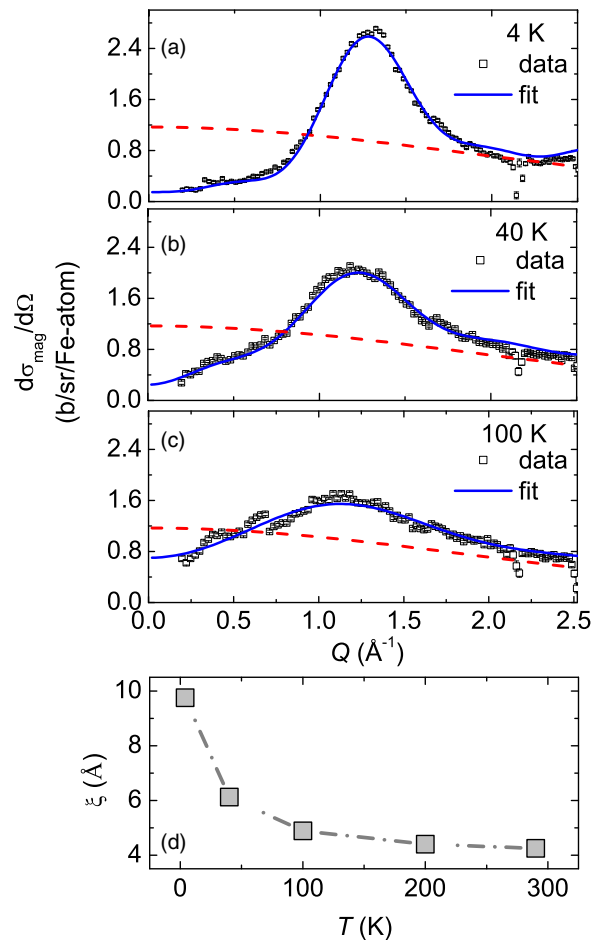

FIG. 5. (Color online) (a)–(c) The magnetic scattering intensity of $FeAl_2O_4$ at 4, 40, and 100 K along with the fit curve (blue solid line) assuming fourth NN (40 K) shell and fifth NN (4 K) shell, following Eq. (1). The red (—) line is drawn proportional to $f^2(\mathbf{Q})$ for Fe^{2+}. Panel (d) shows that the spin-spin correlation length ξ decreases as temperature increases.

both systems are comparable, indicating that the dominant exchange interactions are comparable.

D. Polarized neutron scattering: MnAl$_2$O$_4$

1. Co-existence of short- and long-range spin correlations

The results of polarized neutron-scattering experiment on $MnAl_2O_4$ are presented in Figs. 7 and 8. In Fig. 7(a), the nuclear coherent contribution to the differential scattering cross section at 4 K is shown. The structural model as obtained
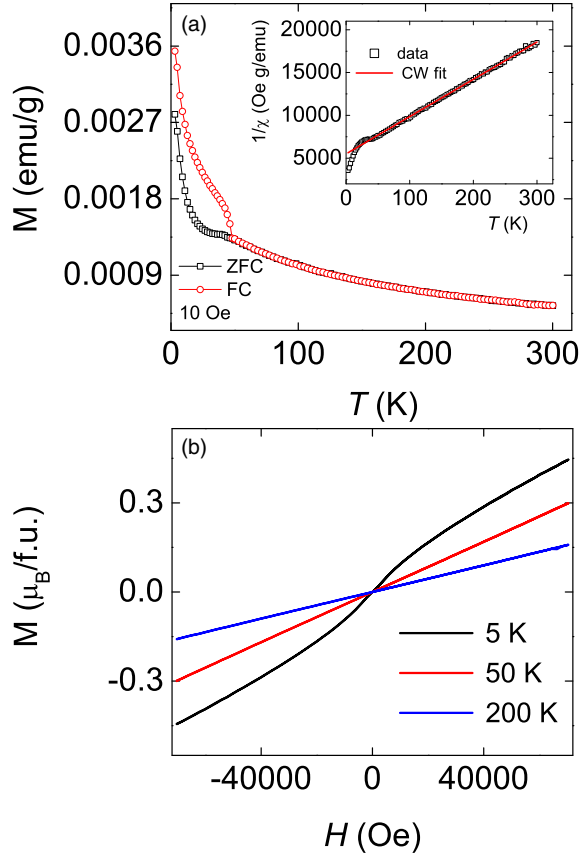
TABLE II. Parameters estimated from fits to magnetic cross section of $FeAl_2O_4$ using Eq. (1). g is the Landé factor, $\frac{\langle S_0 \cdot S_n \rangle}{S(S+1)}$ denotes the spin-spin correlations, and ϵ^2 is an indicator of the goodness of fit, defined such that for the best fit $\epsilon^2 \approx 1$. The parameters [c_n, R_n(Å)] used for the fits, for example at 4 K, are $(c_1, R_1) = (4, 3.53)$; $(c_2, R_2) = (12, 5.77)$; $(c_3, R_3) = (12, 6.76)$; $(c_4, R_4) = (6, 8.15)$; $(c_5, R_5) = (12, 8.89)$; $(c_6, R_6) = (8, 9.9)$. The terms for the third and higher shells are rather insignificant, however they were necessary for a faithful fit.

T (K)	g	$\frac{\langle S_0 \cdot S_1 \rangle}{S(S+1)}$	$\frac{\langle S_0 \cdot S_2 \rangle}{S(S+1)}$	$\frac{\langle S_0 \cdot S_3 \rangle}{S(S+1)}$	$\frac{\langle S_0 \cdot S_4 \rangle}{S(S+1)}$	$\frac{\langle S_0 \cdot S_5 \rangle}{S(S+1)}$	$\frac{\langle S_0 \cdot S_6 \rangle}{S(S+1)}$	ϵ^2
4	2.453(18)	−0.512(20)	0.144(15)	0.013(20)	−0.056(71)	−0.095(37)	0.030(14)	0.985
40	2.435(18)	−0.325(12)	0.056(16)	0.005(18)	0.000(80)	−0.032(16)		0.965
100	2.359(17)	−0.157(12)	0.005(6)					0.933

FIG. 6. (Color online) (a) The ZFC and FC magnetization curves of $MnAl_2O_4$ showing a bifurcation at $T_N \approx 40$ K. The inset shows the Curie-Weiss fit of inverse magnetic susceptibility. Panel (b) shows the magnetic hysteresis at 5, 50, and 200 K.
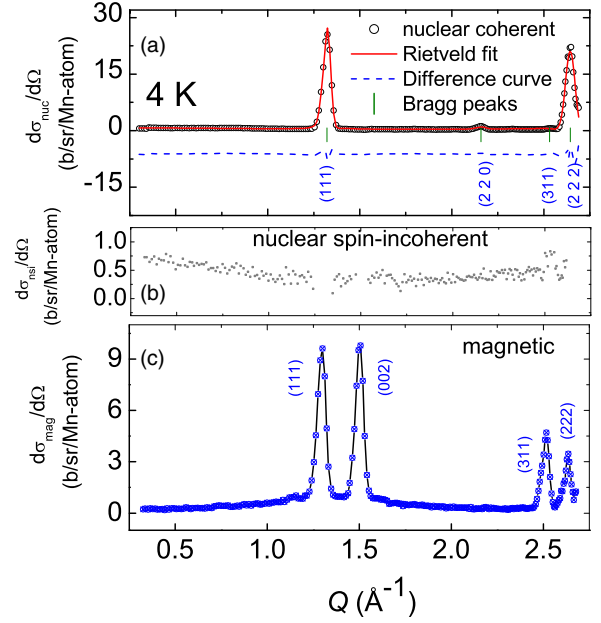

FIG. 7. (Color online) (a) Nuclear coherent contribution to the differential scattering cross section of $MnAl_2O_4$ at 4 K. The results of Rietveld fit in $Fd\bar{3}m$ space group are shown and Bragg peaks are marked. (b) Shows the nuclear spin-incoherent cross section. (c) Shows the indexed magnetic peaks at 4 K. In contrast to $FeAl_2O_4$, long-range order is present at 4 K.

from x-ray powder diffraction yields reasonable agreement, while the DNS instrument is not a dedicated powder diffractometer. Similar to the case of $FeAl_2O_4$, the nuclear-scattering intensity was refined using the $Fd\bar{3}m$ space-group symmetry, as presented in Fig. 7(a) for 4-K data. The nuclear spin-incoherent and magnetic contributions at 4 K are presented in Figs. 7(b) and 7(c) respectively. The separated magnetic intensity exhibits (111) and (222) Bragg peaks and additional peaks at (002) and (311). The magnetic reflections could be indexed using $\mathbf{k} = (000)$ which lead to two possible irreducible representations (IR), Γ_8 and Γ_9 (according to the numbering scheme of Kovalev [24]). Though limited in $\mathbf{Q}$ range, the magnetic scattered intensity was analyzed in Γ_8 representation and the results of the Rietveld refinement are presented in Fig. 7(c) as the indices of magnetic reflections (111), (002), (311), and (222). The magnetic structure suggested by the refinement is schematically represented in Fig. 9. However,

the magnetic moment direction in the case of cubic symmetry cannot be uniquely determined from powder-diffraction data alone [26]. The observed and calculated intensities for (111),
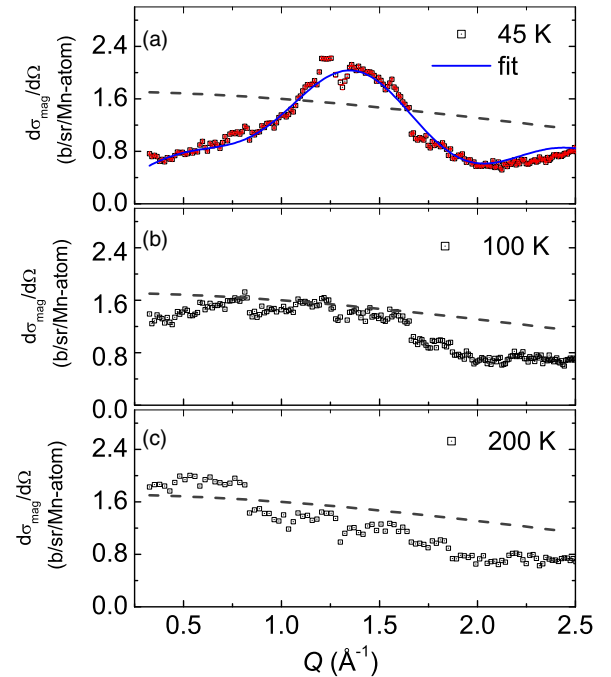

FIG. 8. (Color online) (a)–(c) Magnetic scattering cross sections at 45, 100, and 200 K, respectively. The curve fit according to Eq. (1) for 45 K is shown. The steplike features seen in 200-K data are attributable to inefficient detector calibration. The gray (− −) line is drawn proportional to $f^2(\mathbf{Q})$ of Mn^{2+}.

TABLE III. Spin-spin correlation parameters estimated from the fits to the magnetic cross section of $MnAl_2O_4$ using Eq. (1) for 45-K data.

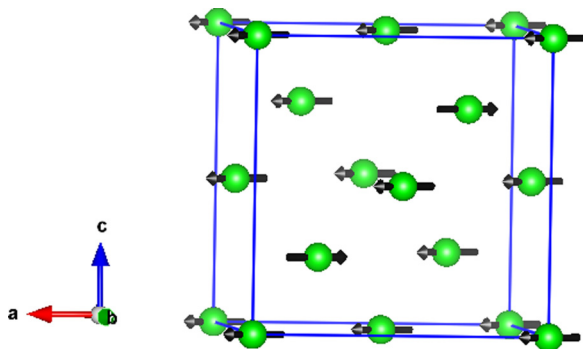| g	$\frac{\langle S_0 \cdot S_1 \rangle}{S(S+1)}$	$\frac{\langle S_0 \cdot S_2 \rangle}{S(S+1)}$	$\frac{\langle S_0 \cdot S_3 \rangle}{S(S+1)}$	ϵ^2
2.110(13)	−0.360(10)	0.166(10)	−0.122(11)	0.953

FIG. 9. (Color online) The magnetic structure of $MnAl_2O_4$. Only the Mn atoms that form the diamond lattice are shown. The figure was created using the software *Balls & Sticks* [25]. Note that the moment direction cannot be determined from neutron powder diffraction for a cubic crystal system.

(002), (311), and (222) reflections are collected in Tables III and IV for a comparison. The average magnetic moment at 4 K visible in the Bragg reflection is refined to a value of $1.17(4)\mu_B$ which is considerably reduced compared to the spin-only saturation moment assuming complete long-range order of the Mn lattice. Roth reported the magnetic structure of $MnAl_2O_4$ where each spin at the A site is surrounded by oppositely aligned nearest-neighbor spins in one tetrahedra [7]. However, Tristan *et al.* [4] point out that the simple collinear picture and the estimated transition temperature of 6.4 K by Roth disagree with the observation of the diminished value of local moment $5\mu_B$ (for a fully ordered spin-only system) and $T_N \approx 40$ K. Thus it is clear that significant magnetic disorder persists down to lowest temperatures. The cation inversion was suggested as the reason where Mn spins at A and B sites build paramagnetic clusters. However, later, by neutron powder-diffraction study the magnetic structure of $MnAl_2O_4$ was deduced as a collinear antiferromagnetic type with $T_N \approx 42$ K [27].

It is clear that the low-temperature magnetic properties of $MnAl_2O_4$ are different from those of $FeAl_2O_4$ as sharp peaks signify long-range magnetic order to emerge below 45 K [Fig. 7(c)]. However, besides sharp peaks due to long-range order, we observe diffuse intensity in the ordered state, which survives above the Néel temperature $T_N \approx 40$ K, centered around $|\mathbf{Q}| \approx 1.3$ Å^{-1}.

At 200 K, the scattered intensity follows more or less the form factor behavior of free magnetic ion Mn^{2+}. The magnetic scattering cross section of $MnAl_2O_4$ at 45, 100, and 200 K is presented in Figs. 8(a)–8(c). The diffuse magnetic intensity observed for $MnAl_2O_4$ at 45 and 100 K were analyzed using

TABLE IV. The observed (F_{obs}^2) and calculated (F_{calc}^2) intensities for the (hkl) reflections presented in Fig. 7(c).

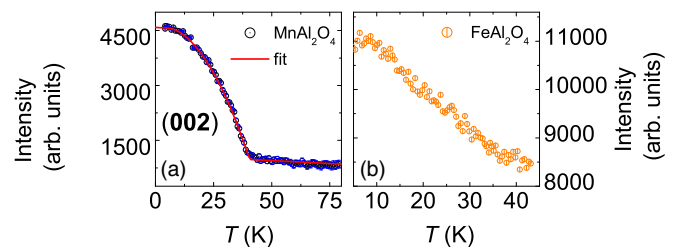| (h k l)	F_{obs}^2	F_{calc}^2	d spacing
(1 1 1)	0.195(2)	0.192	4.75287
(0 0 2)	0.912(2)	0.977	4.11611
(3 1 1)	0.034(4)	0.039	2.48211
(2 2 2)	0.199(3)	0.209	2.37644

FIG. 10. (Color online) (a) The temperature dependence of magnetic intensity of $MnAl_2O_4$, where the magnetic phase transition at $T_N \approx 40$ K is clear. The solid red line shows the fit according to a mean-field model as per Eq. (2). (b) In the case of $FeAl_2O_4$, a linear curve of dominant magnetic fluctuations is observed.

Eq. (1) as was done in the case of $FeAl_2O_4$. The results of the fit are presented in Fig. 8(a) as solid lines and the estimated parameters for 45-K data are presented in Table IV. Inclusion of three NN shells was required to obtain a satisfactory fit. Since Mn^{2+} is an $L = 0$ ion, the deviation from the spin-only value is not significant. Fits were also performed by keeping g constant at the spin-only value, however, it did not lead to significant changes in the parameters. From the refined parameters, $\frac{\langle S_0 \cdot S_1 \rangle}{S(S+1)}$, prominant NN antiferromagnetic and NNN ferromagnetic exchange were concluded, similar to the case of $FeAl_2O_4$. In the case of $FeAl_2O_4$, $\frac{\langle S_0 \cdot S_1 \rangle}{S(S+1)} = -0.325(12)$ at 40 K whereas in the case of $MnAl_2O_4$, it is $-0.360(10)$ at 45 K.

The temperature evolution of the peak intensity of the (002) magnetic reflection of $MnAl_2O_4$ is presented in Fig. 10(a). For this measurement, the detector bank of the DNS instrument was aligned such that the (002) Bragg peak illuminates a specific detector tube and the intensity was recorded as a function of temperature. As such, the detector signal does not represent the integrated but the peak intensity. The angular coverage of a single tube is sufficient to account for the lattice expansion in the respective temperature region. The magnetic intensity sharply decreases around $T_N \approx 40$ K where the magnetic phase transition occurs, however, it can be seen from the figure that even at $T > T_N$, there exists nonzero intensity signifying the presence of magnetic fluctuations. We analyze the temperature evolution in terms of a mean-field approximation, giving the reduced sublattice magnetization [28]

$$M = B_S\left[\frac{3S}{(S+1)}\left(\frac{T_N}{T}\right)M\right], \qquad (2)$$

where M is the magnetic intensity, S is the spin quantum number, and B_S is the Brillouin function. The scattered intensity is proportional to the square of the magnetization. We take the diffuse intensity into account by adding a sloping line. Leaving S a free parameter, the model yields $S = 2.3(2), T_N = 40(1)$ K in agreement with $S = \frac{5}{2}$ for Mn^{2+} and the macroscopic data.

IV. DISCUSSION

Previous reports on magnetic properties of A-site spinels have suggested spin-glass-like and antiferromagnetic ground states, respectively, for $FeAl_2O_4$ and $MnAl_2O_4$ [4,16]. Early reports on the spin-glass phase in $FeAl_2O_4$ were based on experiments performed on samples with relatively significant

degree of cation inversion (for example, 17% reported in [16]). In $FeAl_2O_4$ samples with approximately 8% cation inversion, proximity to spin-glass phase was suggested by Krimmel *et al.* But the reported quadratic T dependence of specific heat of $FeAl_2O_4$ at low temperature is in contradiction with the T-linear response of canonical spin glasses. To explain this discrepancy, an argument based on spin-orbital liquid due to the presence of Jahn-Teller Fe^{2+} in the tetrahedral site was put forward in [4] in comparison with observations on $FeSc_2S_4$ [2] and $FeCr_2S_4$ [3].

Our macroscopic magnetic measurements, ac susceptibility, and *memory effect* test have ruled out a spin-glass scenario in $FeAl_2O_4$ samples with a particularly low degree of cationic inversion. The apparent different behavior of our samples (virtually no cation inversion and no spin-glass behavior) and samples from earlier reports (large cation inversion, interpretation in the framework of the spin-glass scenario) could be due to the additional disorder in the latter samples, which, together with magnetic frustration, could indeed lead to a spin-glass phase, so no unambiguous proof has been given in [1] and [4]. The diffuse magnetic scattering results presented here on $FeAl_2O_4$ are direct confirmation of the predominant short-range order present down to 4 K. The analysis of magnetic scattered intensity shows that the spin-spin correlations in $FeAl_2O_4$ extend up to third-nearest-neighbor shells in the spinel unit cell. It is tempting to interpret the results on Fe, Mn spinels based on the "order by disorder" physics adopted to the case of *A*-site spinels which are diamond-lattice antiferromagnets [6]. In this scenario, frustration is brought about by competition between the nearest- and next-nearest-neighbor interactions, J_1 and J_2, and the magnetic ground state is tuned by the ratio of these values. Accordingly, in the weakly frustrated limit where $0 \leqslant (\frac{J_2}{J_1}) \leqslant \frac{1}{8}$, the magnetic ground state is the Néel phase with antiparallel spins on the NNs. As the value of J_2 increases, the Néel phase transforms to *spiral spin-liquid* phase. Increase in frustration through increase in J_2 also results in the reduction of T_N with respect to Θ_{CW}. In the case of $FeAl_2O_4$, with $\Theta_{CW} \approx 121$ K and $T_a \approx 13$ K, a notable reduction in T_a is clear which suggests the enhancement of J_2. The mean-field exchange parameter J_{MF} reported [1] for $FeAl_2O_4$ is 16.25 K, which lies between those of $MnAl_2O_4$ ($J_{MF} = 12.3$ K) with $(\frac{J_2}{J_1}) \approx 0.09$ and $CoAl_2O_4$ ($J_{MF} = 20.8$ K) with $(\frac{J_2}{J_1}) \approx 0.17$. From these values, it is suggestive that the magnetic ground state evolves from the Néel state in $MnAl_2O_4$ towards spin liquid in $FeAl_2O_4$. This is reflected in the coexistence of long- and short-range order in the Mn spinel and the dominance of short-range spin fluctuations in the Fe spinel in our study. In a detailed neutron-scattering study on a single crystal of $CoAl_2O_4$, MacDougall *et al.* [29] argue that the phase transition observed at 6.5 K shows first-order nature with long-range magnetic order being inhibited by kinetic freezing of domain walls. While such a scenario based on kinetic freezing of domain walls can form the basis for glassylike features observed in some of the *A*-site spinels, our magnetic measurements on $FeAl_2O_4$ show no signatures of glasslike freezing. From the present experimental results it is not possible to verify the presence, if at all, of clusters or domain-related liquidlike distributions which could be modeled by assuming rigid magnetic droplets.

Site inversion, wherein the *A*-site and *B*-site cations exchange their respective crystallographic positions, is an important issue in spinels which has a strong bearing on their magnetic properties. Depending on the degree of inversion, quantified by the inversion parameter x, normal ($x = 0$), random ($x = 2/3$), and inverse ($x = 1$) spinels exist. Through controlled synthesis the degree of inversion can be lowered [4], however a finite amount of disorder exists in real compounds. Previous works on spinels [15,30] have reported the use of different temperatures of synthesis followed by different cooling rates and quenching/annealing procedures to prepare samples with different degrees of inversion. As mentioned in Sec. II, the present set of samples were synthesized at $1000\,°C$ by employing slow rates of cooling in order to obtain a low degree of inversion as suggested by the x-ray studies.

The effect of site inversion on the spin-liquid state of *A*-site spinels has been treated theoretically wherein the effect of weak disorder is found to act as a degeneracy breaking mechanism to select a preferred ground state out of the manifold of available states [31]. The proposed "swiss cheese model" which takes into account the disorder effects shows that the presence of finite amount of disorder does not diminish the frustration effects in an antiferromagnetic diamond lattice. The samples of $FeAl_2O_4$ studied here contain low amounts of disorder, but even in the presence of it, frustration effects assume importance. Recent work on $CoAl_2O_4$ by Roy *et al.* [32] and Hanashima *et al.* [33] have taken into account the important parameter of site inversion to explain the magnetic properties of *A*-site spinels.

In contrast to the case of $FeAl_2O_4$, $MnAl_2O_4$ is in the weakly frustrated regime with evidently an antiferromagnetic phase below T_N. As noted above, a speculative estimation of $(\frac{J_2}{J_1})$ using mean-field approximation [1] and comparison with the theoretical calculations [6] points towards the Néel phase in $MnAl_2O_4$. From our polarized neutron measurements, sharp magnetic peaks are present at 4 K which shows that $MnAl_2O_4$ develops long-range order. Estimation of magnetic moment value through refinement of magnetic scattering data at 4 K leads to a value of $1.17(3)\mu_B/f.u.$. At 5 K, the macroscopically measured magnetic moment under applied field of 50 kOe was $\approx 0.4\mu_B/f.u.$ [see Fig. 6(b)] which is diminished as compared to the spin-only ferromagnetic moment value of Mn^{2+}, $5\mu_B/f.u.$. Through the polarized neutron experiments we prove the existence of short-range order coexisting with long-range ordered regions in the case of $MnAl_2O_4$; see Figs. 10 and 7. In this scenario, where short-range and long-range ordered phases coexist, a magnetic model of spin clusters or kinetically arrested domains suggested in the case of $CoAl_2O_4$ could also account for the features of diffuse magnetic scattering intensity.

V. CONCLUSIONS

To conclude, through polarized neutron-scattering experiments and polarization analysis, we observe predominant short-range order in $FeAl_2O_4$, which extend up to third-nearest-neighbor shells in the spinel unit cell. The contribution from orbital degrees of freedom of Fe^{2+} towards magnetism is suggested. Clear indication of long-range antiferromagnetic order at 4 K is obtained in the case of $MnAl_2O_4$.

However, significant short-range order coexists with long-range magnetic order in this compound even at $T_N \approx 40$ K. A comparison of the magnetic behavior of $MnAl_2O_4$ (Mn^{2+}; $S = \frac{5}{2}$), $FeAl_2O_4$ (Fe^{2+}; $S = 2$), and $CoAl_2O_4$ (Co^{2+}; $S = \frac{3}{2}$) suggests a transition from magnetically long-range order to short-range order as the S value is reduced. This provides a hint for investigating $S = 1$ and $\frac{1}{2}$ spinels in search of quantum effects in spin-liquid states. Through our re-investigation, we have convincingly shown that (i) $FeAl_2O_4$ displays no long-range magnetic order down to 4 K, (ii) the true ground state of minimally disordered $FeAl_2O_4$ is not a canonical spin glass, (iii) in $MnAl_2O_4$, long- and short-range spin correlations coexist. Remarkably, by considering quantum fluctuations as the predominant mechanism that relieves spin frustration, a phase diagram comprising of six coplanar spiral ordering in addition to the Néel phase was suggested [34]. A strong connection between frustration and strength of quantum fluctuations was suggested. However the important role played by the inversion parameter in choosing the magnetic ground state in A-site spinels cannot be discarded.

[1] A. Krimmel, H. Mutka, M. M. Koza, V. Tsurkan, and A. Loidl, Phys. Rev. B **79**, 134406 (2009).

[2] V. Fritsch, J. Hemberger, N. Büttgen, E. W. Scheidt, H. A. Krug von Nidda, A. Loidl, and V. Tsurkan, Phys. Rev. Lett. **92**, 116401 (2004).

[3] R. Fichtl, V. Tsurkan, P. Lunkenheimer, J. Hemberger, V. Fritsch, H.-A. Krug von Nidda, E.-W. Scheidt, and A. Loidl, Phys. Rev. Lett. **94**, 027601 (2005).

[4] N. Tristan, J. Hemberger, A. Krimmel, H.-A. Krug von Nidda, V. Tsurkan, and A. Loidl, Phys. Rev. B **72**, 174404 (2005).

[5] J. Villain, R. Bidaux, J. P. Carton, and R. Conte, J. Phys. **41**, 1263 (1980).

[6] D. Bergman, J. Alicea, E. Gull, S. Trebst, and L. Balents, Nature (London) **3**, 487 (2007).

[7] W. L. Roth, J. Phys. Chem. Solids **25**, 1 (1964).

[8] O. Zaharko, A. Cervellino, V. Tsurkan, N. B. Christensen, and A. Loidl, Phys. Rev. B **81**, 064416 (2010).

[9] R. Mathieu, P. Jönsson, D. N. H. Nam, and P. Nordblad, Phys. Rev. B **63**, 092401 (2001).

[10] W. Schweika and P. Böni, Physica B **297**, 155 (2001).

[11] O. Schärpf and H. Capellmann, Phys. Status Solidi A **135**, 359 (1993).

[12] H. M. Rietveld, J. Appl. Crystallogr. **2**, 65 (1969).

[13] J. Rodriguez-Carvajal, Physica B **192**, 55 (1993).

[14] A. S. Wills, Physica B **276**, 680 (2000).

[15] H. S. O'Neill, W. A. Dollase, and C. R. Ross II, Phys. Chem. Miner. **18**, 302 (1991).

[16] J. L. Soubeyroux, D. Fiorani, E. Agostinelli, S. C. Bhargava, and J. L. Dormann, J. Phys. Colloq. **49**, 1117 (1988).

[17] C. P. Bean and I. S. Jacobs, J. Appl. Phys. **27**, 1448 (1956).

[18] P. Refregier, E. Vincent, J. Hammann, and M. Ocio, J. Phys. **48**, 1533 (1987).

[19] D. S. Fisher and D. A. Huse, Phys. Rev. B **38**, 386 (1988).

[20] J. A. Mydosh, *Spin Glasses: An Experimental Introduction* (Taylor & Francis, London, 1993).

[21] B. D. Rainford, J. Phys. Colloq. **43**, C7 (1982).

[22] P. J. Brown, in *International Tables of Crystallography*, edited by A. J. C. Wilson, Vol. C (Kluwer Academic, Dordrecht, 1995), p. 391.

[23] I. A. Blech and B. L. Averbach, Physics **1**, 31 (1964).

[24] O. V. Kovalev, H. T. Stokes, and D. M. Hatch, eds., *Representations of the Crystallographic Space Groups* (Gordon and Breach, Switzerland, Australia, Belgium, France, 1993).

[25] T. C. Ozawa and S. J. Kang, J. Appl. Crystallogr. **37**, 679 (2004).

[26] G. Shirane, Acta Crystallogr. **12**, 282 (1959).

[27] A. Krimmel, V. Tsurkan, D. Sheptyakov, and A. Loidl, Physica B **378**, 583 (2006).

[28] J. S. Smart, *Effective Field Theories of Magnetism, Studies in Physics and Chemistry* (Saunders, Philadelphia, 1966).

[29] G. J. MacDougall, D. Gout, J. L. Zarestky, G. Ehlers, A. Podlesnyak, M. A. McGuire, D. Mandrus, and S. E. Nagler, Proc. Natl. Acad. Sci. U.S.A. **108**, 15693 (2011).

[30] R. J. Harrison, S. A. T. Redfern, and H. S. C. O'Neill, Am. Mineral. **83**, 1092 (1998).

[31] L. Savary, E. Gull, S. Trebst, J. Alicea, D. Bergman, and L. Balents, Phys. Rev. B **84**, 064438 (2011).

[32] B. Roy, A. Pandey, Q. Zhang, T. W. Heitmann, D. Vaknin, D. C. Johnston, and Y. Furukawa, Phys. Rev. B **88**, 174415 (2013).

[33] K. Hanashima, Y. Kodama, D. Akahoshi, C. Kanadani, and T. Saito, J. Phys. Soc. Jpn. **82**, 024702 (2013).

[34] J. S. Bernier, M. J. Lawler, and Y. B. Kim, Phys. Rev. Lett. **101**, 047201 (2008).